Thermal pressurization during the transition from quasi-static nucleation to dynamic rupture

Stuart V. Schmitt, Eric M. Dunham, Paul Segall *Department of Geophysics, Stanford University*

INTRODUCTION

For decades, researchers have considered shear heating-induced thermal pressurization as a potential dynamic weakening mechanism during earthquakes. In this hypothesis, shear heating pressurizes the pore fluid faster than it can diffuse away, thereby reducing the effective normal stress on the fault.

Recently, researchers have conducted numerical simulations of dynamic rupture that simultaneously solve for coupled heat and pore fluid flow. *Noda, Dunham, & Rice* [JGR, 2009] included thermal pressurization in models of fault rupture with dynamic weakening from flash heating of asperities. In such models, the rupture mode (crack-like or pulse-like) depends strongly on the preexisting stress state on the fault, with pulse-like rupture occurring only on faults with a low background state of shear stress. They found that both thermal pressurization and the nucleation zone dimension also affect the rupture mode. Their nucleation method was artificial; slip initiates in response to an instantaneously imposed stress concentration.

At the same time, *Segall & Rice* [2006] suggested that thermal effects may become dominant during the quasi-static nucleation phase, which is usually modeled using isothermal rate- and state-dependent friction. In the last few years, we have explored that problem further by performing numerical simulations of earthquake nucleation using fully coupled elasticity, friction, and heat/fluid transport. Simulations of "aging law" rate/state-dependent friction coupled to shear heating and heat/fluid transport have shown that, given a realistic hydraulic diffusivity, thermal pressurization dominates frictional weakening at slip speeds of ~0.1 mm/s, which is well before the onset of both seismic radiation and flash heating [*Schmitt, Segall, & Matsuzawa*, JGR, submitted].

In the present work, we attempt to bridge the two studies by extending simulations of thermal pressurization during the nucleation phase into the early stage of dynamic rupture. We use rate/state friction with the aging form of the state evolution law on a zero-width fault.

THERMAL PRESSURIZATION DURING RATE/STATE NUCLEATION

In prior studies, we performed 2D numerical simulations that couple rate/state nucleation with shear heating and diffusive transport of heat and pore pressure. In the absence of thermal pressurization (that is, isothermal and drained), nucleation with the aging state evolution law takes the form of a crack-like slip zone. That is, as slip accelerates, slip in the interior of the nucleation zone accelerates at roughly the same rate as slip at its edges. The stress drop is nearly uniform in the interior of the slip zone and maximum slip occurs at its center.

Thermal pressurization is effectively a slip weakening mechanism that feeds back into itself, and it therefore rapidly dominates in the center of an aging law nucleation zone, where the most slip occurs. This effect leads to dramatic along-strike localization of the nucleation zone at its midpoint (see **Figure 1**). We find that thermal pressurization is weakening with $\dot{\tau} \propto -v^{3/2}$, which cannot be stabilized by reducing the compliance (that is, length) of the nucleation zone.

We quantify the strength of thermal pressurization by defining a critical velocity v_{crit} which corresponds to the maximum slip speed when $|\mu_0 \dot{p}| > |\dot{\mu}(\sigma - p_0)|$ (see **Figure 2**). Using realistic values of hydraulic diffusivity, values of v_{crit} range from 0.02 to 2 mm/s for aging law nucleation. It should be noted that slip law nucleation is pulse-like, and the thermal pressurization effect is therefore reduced because the frictional weakening is predominantly located in an area where little prior slip has occurred.

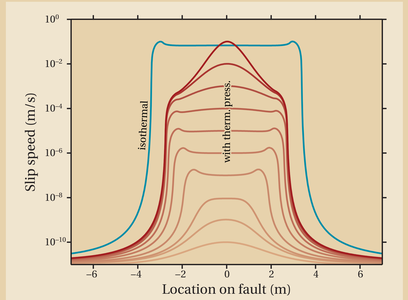

Figure 1. The effect of thermal pressurization on aging law nucleation. Lines are snapshots of slip speed on the fault. In red, snapshots for every 10-fold increase in v_{max} are shown for nucleation with thermal pressurization. The nucleation zone starts as a growing crack, then shrinks. For comparison, the isothermal profile for $v_{\text{max}} = 10^{-1}$ m/s is shown; crack growth continues in this case.

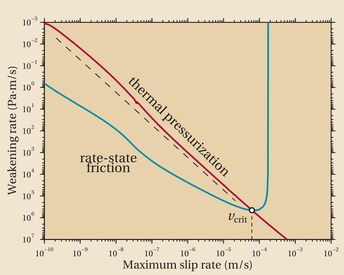

Figure 2. Critical velocity v_{crit}. The two weakening terms $|\mu_0 \dot{p}|$ and $|\dot{\mu}(\sigma - p_0)|$ (summed along the slipping zone) are plotted against v_{max}. Rate/state friction dominates the weakening until $v_{\text{crit}} = 0.06$ mm/s, at which point thermal pressurization becomes the dominant weakening term in the equation of motion.

By the time $v_{\text{max}} = 0.2$ mm/s, thermal pressurization becomes the *only* weakening term. Rate/state friction becomes strengthening because of its direct velocity strengthening component (the a term in eq. [1]).

The dashed line is a reference line with slope 3/2.

GOVERNING EQUATIONS

Rate- and state-dependent friction:

$$\tau = \left[\mu_0 + a \ln \frac{v}{v_0} + b \ln \frac{\theta v_0}{d_c} \right] (\sigma - p) \,. \tag{1}$$

Aging state evolution law:

$$\frac{d\theta}{dt} = 1 - \frac{v\theta}{d_c} \,. \tag{2}$$

Equation of motion:

$$\tau = \tau_0 - \frac{G}{2v_s} v + \phi(x,t) \,. \tag{3}$$

Elastic stress interaction:

$$\phi(x,t) = \int_0^t \int_{-\infty}^{\infty} K(x\text{–}x', t\text{–}t') u(x',t') \, dx' \, dt' \,. \tag{4}$$

Thermal diffusion and shear heating on the fault:

$$\frac{\partial T}{\partial t} = c_{\text{th}} \frac{\partial^2 T}{\partial y^2} \qquad \text{and} \qquad \left. \frac{\partial T}{\partial y} \right|_{y=0} = -\frac{\tau v}{2 \rho c_v c_{\text{th}}} \,. \tag{5}$$

Pore pressure generation and transport:

$$\frac{\partial p}{\partial t} = c_{\text{hyd}} \frac{\partial^2 p}{\partial y^2} + \Lambda \frac{\partial T}{\partial t} \qquad \text{with} \qquad \Lambda = \frac{\Lambda_f - \Lambda_\phi}{\beta_f + \beta_\phi} \,. \tag{6}$$

Table of parameters

G	shear modulus	10 GPa
v_s	s-wave velocity	3700 m/s
μ_0	nominal friction	0.6
a	friction velocity effect	0.012
b	friction state effect	0.015
d_c	slip weakening distance	100 μm
c_{th}	thermal diffusivity	10^{-6} m^2/s
c_{hyd}	hydraulic diffusivity	10^{-6} m^2/s
ρc_v	density × heat capacity	2.86 MPa/°C
Λ	thermal coupling param.	0.8 MPa/°C
K	static or dynamic elastic kernel	
θ	frictional state	
v	slip speed	
u	slip	
T	temperature (change)	
p	pore pressure (change)	
σ	normal stress	
τ	shear stress	
λ_f	pore fluid expansivity	
λ_φ	pore expansivity	
β_f	pore fluid compressibility	
β_φ	pore compressibility	

DESCRIPTION OF MODEL & METHODS

We initiate the simulation using a quasi-static nucleation code [*Schmitt & others*, submitted]. Shortly before seismic radiation becomes significant, we switch to an elastodynamic code [*Noda & others*, 2009]. Apart from the elastic stress interaction term, both codes solve the same governing equation on the same geometry. Features in common include:

- 2D finite difference diffusion grid.
- Periodic boundary condition at fault edges.
- Shear heating included as a boundary condition.
- Driven by constant remote stress rate.

Features of the quasi-static code:

- Started below steady state ($v\theta/d_c < 1$).
- Integrates time derivative of eqs. (1) and (3).
- Grid refinement as accuracy demands.
- Elastic stress interaction calculated in Fourier domain.

Features of elastodynamic code:

- Solves DAE given by eqs. (1) and (3).
- Adaptive substepping for diffusion during elastic steps.
- Spectral boundary integral equation method.

RESULTS

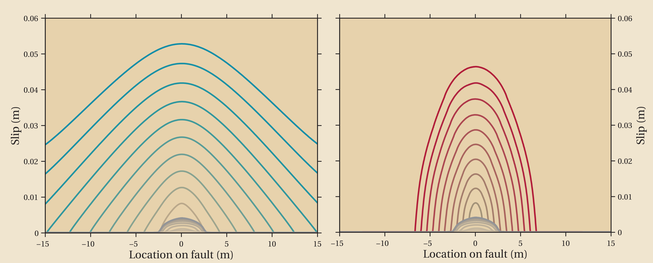

Figure 3. Snapshots of slip. The left plot shows output of a quasi-dynamic simulation, while the right plot includes elastodynamic effects. The snapshots correspond to similar times (see **Fig. 4**).

The rupture propagation velocity in the quasi-dynamic simulation is ~2.5 times larger than in the elastodynamic case. Also, in the quasi-dynamic case, the rupture crack tips rapidly traverse the "preslipped" nucleation zone, whereas elastodynamics restrict that initial rapid crack growth.

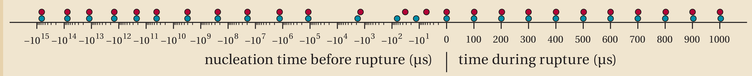

Figure 4. Snapshot times for all figures: quasi-dynamic in blue and elastodynamic in red. The first 14 snapshots are chosen to show tenfold increases in slip speed during nucleation, while the snapshots during the rupture are nearly equally spaced in time.

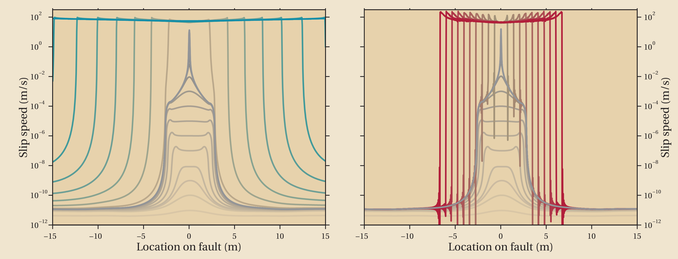

Figure 5. Snapshots of slip speed. In both simulations, nucleation initiates at low slip speed as a localized region of the fault accelerates. At $v \approx 10^{-9}$ m/s, a growing crack forms. Then, when $v = v_{\text{crit}} \approx 10^{-4}$ m/s, thermal pressurization dominates and slip localizes dramatically. Slip accelerates toward instability in a vanishingly tiny nucleation zone. Finally, a seismic rupture initiates at the nucleation location.

The ringing artifacts in the elastodynamic simulation are a consequence of coarse discretization along the fault, which causes the spectral method to be unable to resolve large stress drops. The along-fault discretization was chosen to be computationally inexpensive for the rupture phase but to have sufficient resolution for the nucleation phase.

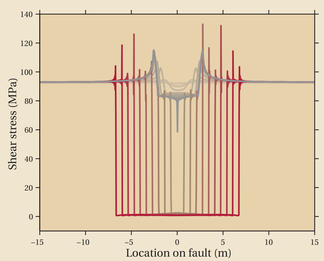

Figure 6. Snapshots of shear stress in the elastodynamic simulation. The site of localized slip resulting from thermal pressurization undergoes a near total stress drop. The total stress drop persists into the seismic rupture.

We note that the high stress state that allows for such a large stress drop is a consequence of the uniform nature of both the material properties and the loading conditions of the system.

CONCLUSIONS

Our preliminary simulations successfully modeled earthquake nucleation and the initiation of seismic rupture, taking into account the effect of thermal pressurization at all phases.

A striking result of our simulations is the near-total stress drop associated with thermal pressurization. If this truly happens, it remains an open question how natural earthquakes have stress drops smaller than expected crustal values of $\sim \mu_0(\sigma - p)$. Perhaps earthquakes nucleate in small high-stress regions and propagate into low-stress regions. However, this idea is possibly incompatible with the notion that very small earthquakes have similar stress drops to large earthquakes.

Much basic work remains. We need to explore the nucleation-to-rupture transition for slip law friction. We have found that the *Linker & Dieterich* [1992] effect of varying normal stress on frictional state mitigates the slip localization; this effect is not included here. Also, correctly modeling thermal pressurization requires accounting for the finite width of the slip zone.